



This open access document is published as a preprint in the Beilstein Archives with doi: 10.3762/bxiv.2019.80.v1 and is considered to be an early communication for feedback before peer review. Before citing this document, please check if a final, peer-reviewed version has been published in the Beilstein Journal of Organic Chemistry.

This document is not formatted, has not undergone copyediting or typesetting, and may contain errors, unsubstantiated scientific claims or preliminary data.

Preprint Title Synthesis of 9-phenylcarbazole hyper-cross-linked polymers in different conditions and adsorption behavior for carbon dioxide

Authors Dandan Fang, Xiaodong Li, Meishuai Zou, Xiaoyan Guo and Aijuan Zhang

Publication Date 30 Jul 2019

Article Type Full Research Paper

ORCID® iDs Meishuai Zou - <https://orcid.org/0000-0002-3608-4088>

Synthesis of 9-phenylcarbazole hyper-cross-linked polymers in different conditions and adsorption behavior for carbon dioxide

Dandan Fang, Xiaodong Li, Meishuai Zou*, Xiaoyan Guo, Aijuan Zhang

School of Materials Science & Engineering, Beijing Institute of Technology, Beijing 100081, China

Email: Meishuai Zou - zoums@bit.edu.cn

Abstract

To systematically explore the effects of the synthesis conditions on the porosity of hyper-cross-linked polymers (HCPs), a series of 9-phenylcarbazole HCPs (P1-P11) have been made by changing the dosage of cross-linker, the reaction temperature, catalyst usage and solvent dosage. Fourier transform infrared spectroscopy is utilized to characterize the structure of the obtained polymers. The TG analysis shows a high thermal stability of the HCPs. More importantly, comparative studies on the porous properties reveals that: molar ration of cross-linker and building block is the main factor of BET specific surface area; Improving reaction temperature or the usage of catalyst could increase the total pore volume greatly but sacrifice part of BET specific surface area; Fortunately changing solvent dosage could remedy this situation, that is slightly changing solvent dosage could simultaneously obtain high surface area and high total pore volume. The BET specific surface areas of P3 is up to $769 \text{ m}^2\text{g}^{-1}$ with narrow pore size distribution and the CO_2 adsorption capacity of P11 is up to $52.4 \text{ cm}^3\text{g}^{-1}$ (273 K/1.00 bar).

Keywords

9-phenylcarbazole; carbon dioxide adsorption; microporous; hyper-cross-linked polymers; synthesis conditions

Introduction

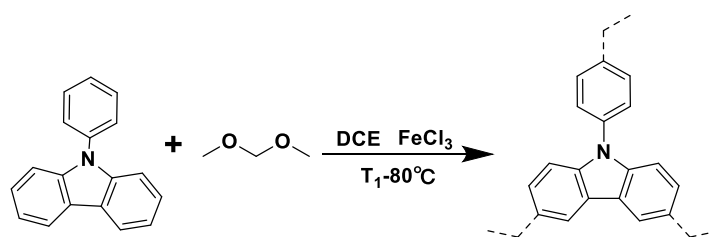
HCPs is a more and more prevalent material due to its high BET specific surface area [1], mild reaction condition [2], non-precious materials catalyst [3] and wide applications [4-6] etc. The synthesis methods of HCPs are also diverse which include solvent knitting methods [7], Scholl coupling reaction [8], the knitting method with FDA [9], functional group reaction [2, 10] and so on. Among these methods, the knitting method with FDA as external cross-linker is the most time-efficient approach [11]. FDA first used as cross-linker to knit aromatic building blocks [12]. Then knitting triptycenes [13], triphenylphosphine [4], benzimidazole [14], carbazole [15], 1,3,5-triphenylbenzene [14], naphthol-based monomers [7] etc. with FDA to obtain sundry HCPs, those HCPs exhibit outstanding porous properties.

The study of the effects on porous properties of HCPs is significant, but almost all the reported focused on the role of monomer length and geometry on porous structure [6, 16-29]. Han has made a series of carbazole-based microporous polymers, reached the conclusion that 2D and 3D conjugated architectures with non-planar rigid conformation and dendritic building blocks is favorable for getting high BET specific surface area [6, 16-18, 20-22]. Qiao synthesized five microporous materials using carbazole with different flexible chain, proving that the flexible chain length is an important factor on the porous properties [23]. Different phenyl-based structures are

also synthesized to explore the monomer structure effect on the porosity [24-29]. Researchers seldom care about the effect of reaction conditions in the synthesis procedure, which is far-reaching significance in preparation of Hyper-cross-linked polymers.

In this work, a series of polymers were synthesized from 9-phenylcarbazole (9-PCz) with FDA as the external cross-linker, tune the porosity by adjusting the reaction condition such as the molar ratio of building unit to cross-linker, the reaction temperature, the catalyst usage and the dosage of solvent. Additionally, the adsorption capacity for carbon dioxide of the obtained polymers was explored.

Results and discussion



Scheme 1: Synthetic route to HCPs

The synthetic illustration of HCPs is depicted in Scheme 1 and Table 1. Using Friedel-Crafts reaction, 11 samples (P1-P11) have been made by changing the molar ratio of building unit to cross-linker (P1-P5), the reaction temperature (P3, P6, P7), the catalyst usage (P3, P8, P9), the dosage of solvent (P3, P10, P11) to study the effect of synthesis conditions on the porosity.

Table 1: Reaction conditions for HCPs

HCPs	9-PCz/mmol	FDA/9-PCz	FeCl ₃ /g	DCE/mL	T/°C
P1	2	1	0.64	18	rt-80

P2	1	2	0.64	18	rt-80
P3	0.67	3	0.64	18	rt-80
P4	0.5	4	0.64	18	rt-80
P5	0.4	5	0.64	18	rt-80
P6	0.67	3	0.64	18	40-80
P7	0.67	3	0.64	18	50-80
P8	0.67	3	0.48	18	rt-80
P9	0.67	3	0.80	18	rt-80
P10	0.67	3	0.64	15	rt-80
P11	0.67	3	0.64	20	rt-80

FT-IR spectrum

FT-IR spectrum was obtained to verify the structure of HCPs shown in Figure 1. The peak at 3100-3000 cm^{-1} correspond to the C-H stretching vibrations of aromatic ring, which declined obviously in P1-P11 compared to monomer 9-PCz. While C-H stretching vibrations of methylene at about 2920 cm^{-1} only emerge in HCPs [9]. What's more, the peak of bisubstituted phenyl ring in 9-PCz monomer at near 725 cm^{-1} deceases while the peak of trisubstituted phenyl ring at near 800 cm^{-1} is dominant in polymers [17]. All of these confirm the reaction of 9-PCz and FDA to form HCPs.

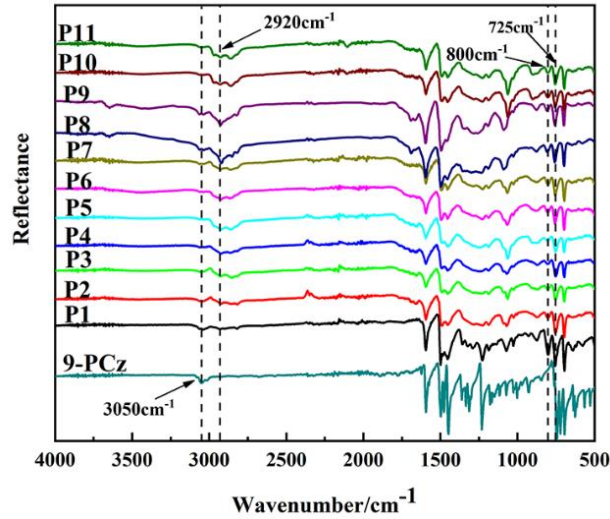


Figure 1: FT-IR spectrum of HCPs and 9-PCz

TG analysis

The TG test were carried out to obtain the thermal stability of HCPs shown in Figure 2, The TG curves of P2, P4, P5, P7 appear a slight drop after 100 °C which is due to the solvent wrapped in the hyper-cross-linked networks and could not be removed even in vacuum [13]. Except this, the TG curves of P1-P11 exhibit the similar decomposition behavior. The highest decomposition temperature of P1-P11 is up to 594 °C and there is ca. 70 % mass residues even the temperature up to 800 °C (Table 2), demonstrating splendid thermal stability as reported microporous polymers [30].

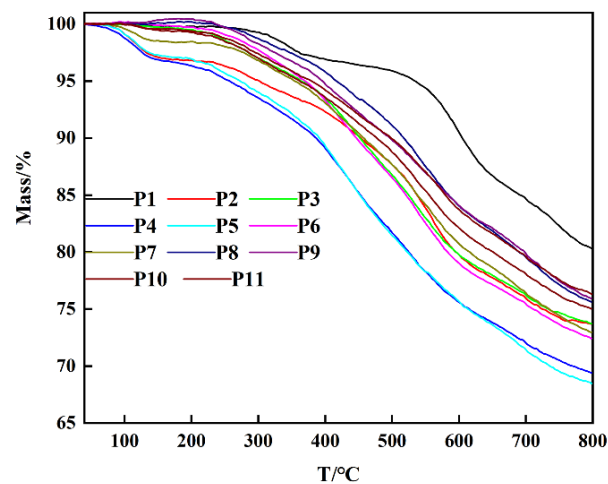


Figure 2: TG curves of HCPs

Table 2: The thermal stability of HCPs

HCPs	Decomposition temperature ^a /°C	Mass residues/%
P1	594	80
P2	301	74
P3	364	74
P4	274	69
P5	273	68
P6	370	72
P7	354	73
P8	417	75
P9	396	76
P10	380	76
P11	362	75

^aDecomposition temperature is the 5 wt% weight loss temperature for HCPs

Morphology analysis

The morphology of P1-P11 was investigated by SEM images in Figure 3 which show that HCPs were composed of rough surface particles. The particles have different size and agglomerate to loosed agglomerates. There are plentiful pores randomly distributed among the particles. The X-ray diffraction (XRD) of obtained HCPs exhibit similar diffraction patterns, only a round peak at 10 °, hinting that P1-P11 are amorphous polymers [9] (Figure 4).

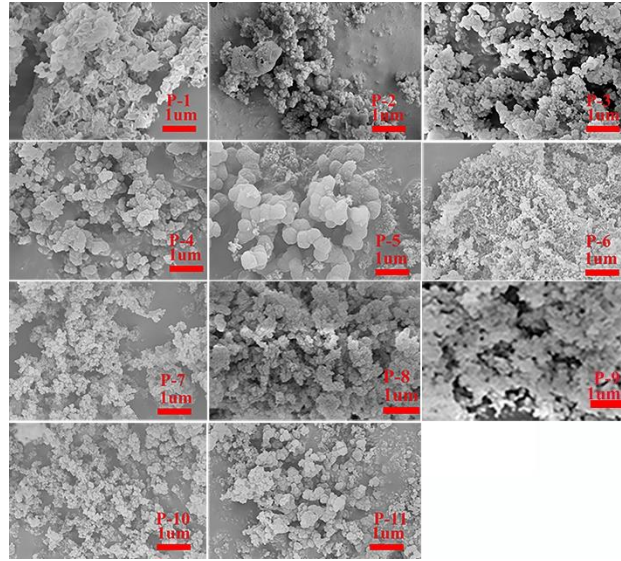


Figure 3: Scanning Electron micrograph of HCPs

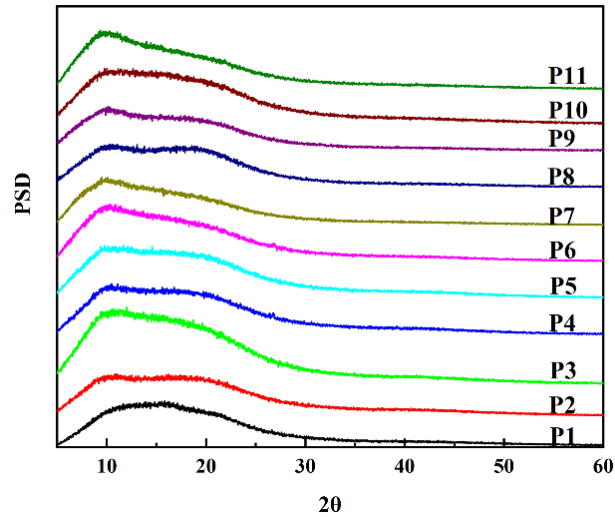


Figure 4: The XRD curves of HCPs

Porous properties

The permanent porous nature was subsequently studied by subjecting the polymers to nitrogen adsorption-desorption experiments at 77 K. The nitrogen adsorption-desorption isotherm and pore size distribution (PSD) curves of P1-P11 displayed in Figure 5 and the porosity data listed in Table 2.

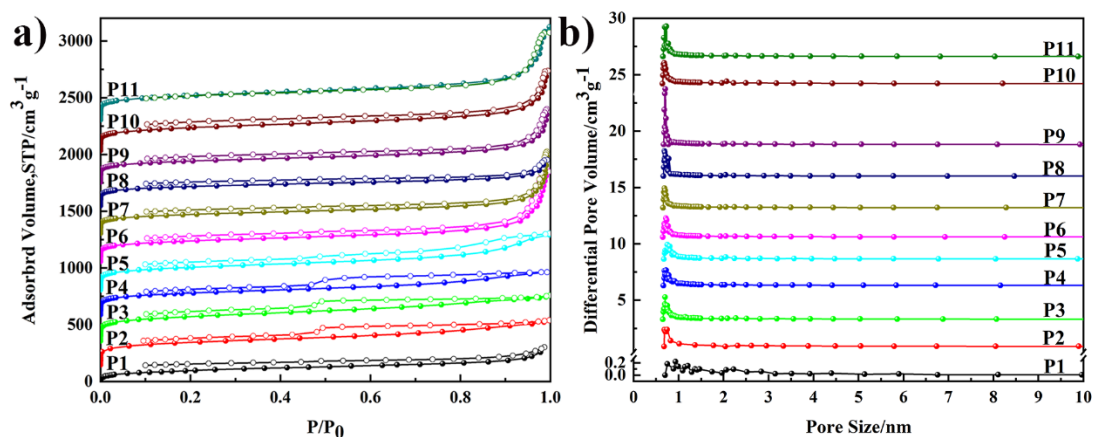


Figure 5: Nitrogen sorption isotherms (a) and pore size distribution (b) of HCPs

Table 3: Porosity data for HCPs

HCPs	S_{BET}^a/m^2g^{-1}	S_{micro}^b/m^2g^{-1}	SA_{lang}^c/m^2g^{-1}	V_{total}^d/cm^3g^{-1}	V_{micro}^e/cm^3g^{-1}
P1	350	0	481	0.47	0
P2	709	311	970	0.62	0.14
P3	769	331	1049	0.63	0.14
P4	696	322	926	0.59	0.14
P5	721	319	965	0.76	0.14
P6	659	286	880	1.24	0.13
P7	599	271	800	1.12	0.12
P8	612	328	821	0.64	0.15
P9	671	336	890	1.00	0.15
P10	755	334	1013	1.11	0.15
P11	760	343	1025	1.27	0.15

^{a, d} surface area and pore volume were obtained by Brunauer-Emmett-Teller (BET)

method between the pressure range of 0.05-0.35 P/P_0 ; ^b Microporous surface area

calculated from the adsorption branch of the nitrogen adsorption-desorption isotherm using the t -plot method; ^c Surface area calculated from the nitrogen adsorption branch based on the Langmuir model; ^e microporous volume calculated from the adsorption branches using NLDEF methods.

The effect of cross-linker dosage (P1-P5)

The reaction condition of P1-P5 is similar expect the gradually increasing proportion of FDA/9-PCz from 1 to 5. The sorption isotherm of P1-P5 (Figure 5a) showed great difference, expect P1, P2-P5 exhibit a rapid nitrogen adsorption ability at the low pressures ($P/P_0 < 0.05$) which belong to the microporous materials [31]. Hysteresis tend to be more obvious for P2-P4 between adsorption and desorption, indicating that the networks contain mesopores [32]. The sorption isotherm of P2-P4 exhibit a combination of type I and IV nitrogen sorption isotherms according to the IUPAC classification [33]. There is no sharp rise at high relative pressures above 0.9 of P1-P5 indicating the scarcely macropores [34]. In addition, the pore size distribution (PSD, Figure 5b) shows that P2-5 exhibit narrow pore size distribution, with the peaks appeared mainly in the micropore scopes (< 2 nm). While P1 has a wide pore size distribution. The porosity parameters are summarized in Table 3. The surface areas of P1-P5 range from 350 to 769 m^2g^{-1} . The lowest specific surface area of P1 is due to the low crosslinking density for less FDA. While largely exaltation BET surface area from P1 to P3 is due to that the crosslinking density increased with the increasing FDA/9-PCz ratio, but further increasing the FDA usage could not get higher BET specific surface area, because the high steric hindrance prevents further crosslinking

reaction [35]. All that reveal that enough and suitable cross-linker usage is the premise of superior specific surface areas, so P3 exhibits the best porous properties.

The effect of reaction temperature (P3, P6, P7)

Based on the selected P3, improving reaction temperature to 40, 50 °C got P6 and P7. The Nitrogen sorption isotherms study of P3, P6, P7 showed in Figure 5. Compare and contrast the sorption isotherm of the HCPs, it is easy to find that P6, P7 show a combination of type I and II nitrogen sorption isotherms as emerging two steep N₂ adsorption ability at low pressure region ($P/P_0 < 0.1$) and high pressure region ($P/P_0 > 0.9$), indicating that micropores and macropores appear in the polymers [36]. The porosity of P3 has been discussed above. The BET specific surface area of P3, P6 and P7 ($769 \text{ m}^2\text{g}^{-1}$, $659 \text{ m}^2\text{g}^{-1}$ and $599 \text{ m}^2\text{g}^{-1}$ respectively) decreased with increasing temperature, microporous surface area and the microporous volume present the same trend, but the total pore volume ($0.63 \text{ cm}^3\text{g}^{-1}$, $1.24 \text{ cm}^3\text{g}^{-1}$ and $1.12 \text{ cm}^3\text{g}^{-1}$ respectively) increased heavily. This may be the result of that excessive temperature cause excessive crosslink at the beginning reaction, the plethora network cocooned part of reaction center, prevented it from further cross-linking (micropores), but formed macropores. All that indicate that improving reaction temperature could enhance the total pore volume of HCPs but lower the specific surface area.

The effect of catalyst usage (P3, P8, P9)

To explore the catalyst usage effect on the HCPs porosity, P8 (3 mmol FeCl₃) and P9 (5 mmol FeCl₃) were made by changing the catalyst usage of P3 (4 mmol FeCl₃). The Nitrogen sorption isotherms of P8, P9 is similar as P7, means that the polymers

simultaneously exist micropores and macropores. The specific surface area for P8 ($612 \text{ m}^2\text{g}^{-1}$) and P9 ($671 \text{ m}^2\text{g}^{-1}$) is inferior to P3 ($769 \text{ m}^2\text{g}^{-1}$), but the total pore volume of P9 ($1 \text{ cm}^3\text{g}^{-1}$) is much higher than P3 ($0.63 \text{ cm}^3\text{g}^{-1}$), P8 ($0.64 \text{ cm}^3\text{g}^{-1}$). The influence of catalyst usage on the porosity could conclude that suitable catalyst usage could get high specific surface area, but further improving the catalyst usage could get high pore volume which may be harmful to the specific surface area.

The effect of solvent dosage (P3, P10, P11)

The different dosage of 1,2-dichloroethane (DCE, 15 ml, 18 ml and 20 ml) was used in the preparation of P3, P10 and P11. The porosity of these HCPs is show in Figure 5 and Table 3. The sorption isotherm of P10 and P11 is similar as P7, signifying the presence of permanent micropores and macropores in the polymers [2]. While P3 porosity is composed of micropores and mesopores as above-mentioned. The PSD of the three HCPs bears resemblance, showing narrow distribution in micropores region and pore size center at ca. 0.7 nm. the BET specific surface area of P3, P10, P11 is about the same ($769 \text{ m}^2\text{g}^{-1}$, $755 \text{ m}^2\text{g}^{-1}$, $760 \text{ m}^2\text{g}^{-1}$ respectively), the microporous surface area and the microporous volume also is similar. However, there are wide disparities in total pore volume among the obtained polymers. The total pore volume of P3, P10 and P11 is $0.63 \text{ cm}^3\text{g}^{-1}$, $1.11 \text{ cm}^3\text{g}^{-1}$ and $1.27 \text{ cm}^3\text{g}^{-1}$ respectively. The volume of P10, P11 is about twice that of P3 which is owing to the extra generated macropores of P10, P11. We conjecture the concentration of reaction system could affect formation process of polymers and its morphology when polymers particles agglomerate and stack together (Figure 3), therefore there is macropores in P10 and

P11. It could reach conclusion that slightly changing of solvent dosage could increase the pore volume greatly without sacrificing the BET special surface area.

Adsorption behaviour of CO₂

The presence of rich CO₂-philic sites (N atom) and narrow pore distribution in networks could improve the molecular interaction with CO₂ [18]. Hence, three polymers (P3, P10, P11) were picked out as representatives to conduct CO₂ adsorption up to 1 bar at both 273 and 298 K (Figure 6a). HCPs get a similar and moderate CO₂ uptake (Table 4). P11 displays the optimal CO₂ storage of 52.4 cm³g⁻¹ (10.4 wt%) at 1.0 bar/273 K. which is higher than the carbazole based microporous polymers PBT-C1 (46 cm³g⁻¹) [23], CMPSO-1B3 (46.8 cm³g⁻¹) [21], CPOP2-4 (7.8-9.0 wt%) [16], tetraphenyl methane based CPOP10 (S_{BET}=3337 m²g⁻¹, 9.1 wt%, at 298 K/1.00 bar) [37], melamine based microporous PAN-NH-NH₂ (9.7 wt%) [30]. There is no saturation appeared when the pressure reached to 1 bar, signifying a higher CO₂ capacity can be obtained by improving the pressure. The isosteric heat (Q_{st}) of each polymers was calculated based on the adsorption data at different temperature using Clausius–Clapeyron equation (Figure 6b), at the zero CO₂ gas surface coverage, the limiting enthalpies of adsorption of three samples is similar (P3:30 kJ/mol, P10:28 kJ/mol, P11:29 kJ/mol) and within the scope of physical adsorption [38], which is beneficial to reuse of materials.

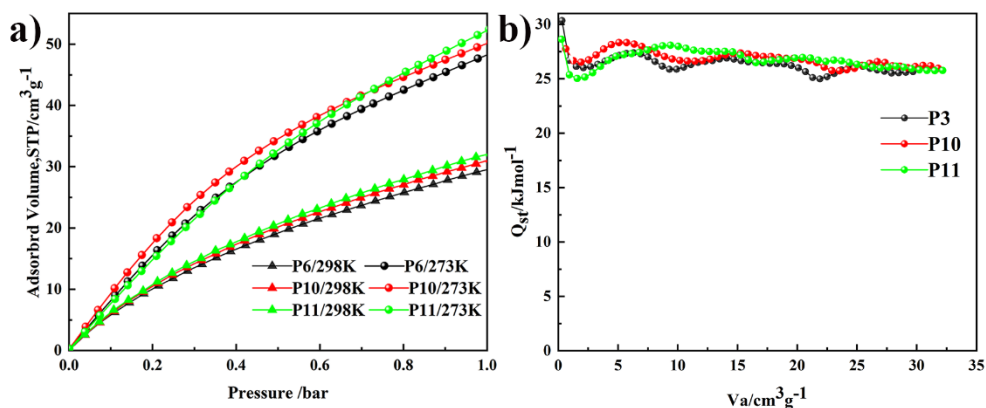


Figure 6: Volumetric CO₂ adsorption isotherms up to 1 bar (a) and the isosteric heat curves of HCPs (b).

Table 4: CO₂ adsorption of HCPs

Samples	CO ₂ uptake/cm ³ ·g ⁻¹		Q _{st} /kJ·mol ⁻¹
	273K	298K	
P3	48.5	29.7	30
P10	50.3	31.2	28
P11	52.4	32.2	29

Conclusion

Using Friedel-Crafts reaction, 9-PCz microporous polymers (P1-P11) prepared by changing the molar rate of cross-linker and building block (P1-P5), the reaction temperature (P3, P6, P7), the usage of catalyst (P3, P8, P9) and the dosage of solvent (P3, P10, P11). The systematic study focused on the porosity shows that the molar ratio of cross-linker and building block is the main influence of BET specific surface area, enough cross-linker is the premise of superior BET specific surface areas;

Improving reaction temperature or catalyst usage could increase the pore volume greatly but sacrifice part of BET specific surface area. Fortunately changing solvent dosage could remedy this situation, that is slightly changing solvent dosage could simultaneously obtain high surface area and high total pore volume. This provides a reference for preparing HCPs with high BET specific surface area and total porous volume using the same one monomer by Friedel-Crafts reaction. The BET specific surface area of the prepared HCPs is up to $769 \text{ m}^2\text{g}^{-1}$, and the CO_2 uptake capacity is up to 10.4 wt% at 273 K/1bar.

Experimental

Materials

9-phenylcarbazole, FDA and DCE were purchased from Aladdin Chemical Reagent Corp. (Shanghai, China). FeCl_3 were acquired from the Macklin Chemical Reagent Ltd Co. (Shanghai, China). Methanol, THF, HCl, and distilled water were obtained from TONG GUANG Fine Chemicals Company. (Beijing, China). Unless stated otherwise, all the solvents and chemicals were used without further purification.

Characterization Methods

Fourier transform infrared (FT-IR) spectra of HCPs were obtained by using a Nicolet 6700 spectrometer over a wavenumber range of $4000\text{-}400 \text{ cm}^{-1}$ by scanning 32 times at a resolution of 4 cm^{-1} . TG analysis of polymers were conducted with a NETZSCH TG 209F1 TG analyzer for $40\text{-}800 \text{ }^\circ\text{C}$ at a heating rate of $10 \text{ }^\circ\text{Cmin}^{-1}$ under nitrogen flows of 50 mLmin^{-1} . The X-ray diffraction (XRD) patterns of the as prepared polymers were collected using a PANalytical X'pert Pro MPD diffractometer with

Cu-K α radiation at room temperature, with step size of 0.0202°, 2 θ ranging from 5.0 to 60°. Scanning electron microscope (SEM) measurements of obtained samples were carried out using a Hitachi SU1510 microscope. The nitrogen adsorption and desorption and the CO₂ adsorption and desorption isotherms of HCPs were obtained using a GAPP V-Sorb 2800P BET surface area and pore volume analyzer. Polymers were degassed at 100 °C for over 10 h under vacuum before all gas analysis.

Synthesis HCPs

The synthetic illustration of HCPs is depicted in Scheme 1. Using Friedel-Crafts reaction, P1-P11 have been made by changing the molar ratio of building unit to cross-linker (P1-P5), the reaction temperature (P3, P6, P7), the catalyst usage (P3, P8, P9) and the dosage of solvent (P3, P10, P11). Synthesis of P3 as representative procedure is given in details: Under a nitrogen atmosphere, 9-PCz (0.67 mmol, 0.163 g), FDA (2 mmol, 0.152 g) was dispersed in DCE (18 mL), and then anhydrous FeCl₃ (4 mmol, 0.64 g) was added to the solution; the mixture was allowed to react at room temperature for 5 h, then 80 °C for 19 h by vigorously stirring. After cooling to room temperature, the solid product was quenched by using 20 mL of CH₃OH, washed several times with Methanol, THF, HCl-H₂O (v/v=2:1) and distilled water, further purified by Soxhlet extractor with ethanol for 24 h and THF for another 24 h. finally dried in a vacuum oven at 100 °C for 24 h. The obtained polymer material was brown solid.

The synthesis of other polymers was similar as P3, only changed the dosage of reaction monomer or experimental conditions as table 1. Although washed excessively,

the yield of the polymers still exceeded 100 % which was due to the adsorbed catalyst or solvent in the pore structure [15]. All obtained samples were colored ranging from pale brown to dark brown.

Acknowledgements

The characterization studies were supported by Advanced Materials Experimental Center, Beijing Institute of Technology.

References

1. Li B.; Guan Z.; Wang W. *Advanced Materials*, **2012**, *24*, 3390-3395.
2. Sekerová L.; Lhotka M.; Vyskočilová E. *Chemistry – A European Journal*, **2018**, *24*, 14742-14749.
3. Chaoui N.; Trunk M.; Dawson R. *Chemical Society Reviews*, **2017**, *46*, 3302-3321.
4. Xu C.; Wang H.; Wang Q. *Applied Surface Science*, **2019**, *466*, 193-201.
5. Liang H.-P.; Chen Q.; Han B.-H. *ACS Catalysis*, **2018**, *8*, 5313-5322.
6. Zhang W.; Tang J.; Yu W. *ACS Catalysis*, **2018**, 8084-8091.
7. Dawson R.; Stevens L. A.; Drage T. C. *Journal of the American Chemical Society*, **2012**, *134*, 10741-10744.
8. Zhu X.; Tian C.; Jin T. *ACS Macro Letters*, **2017**, *6*, 1056-1059.
9. Hou S.; Tan B. *Macromolecules*, **2018**, *51*, 2923-2931.
10. Zhu T.; Xie F.; Huang T. *ACS Macro Letters*, **2018**, *7*, 1283-1288.
11. Hou S.; Razzaque S.; Tan B. *Polymer Chemistry*, **2019**, *10*, 1299-1311.
12. Li B.; Gong R.; Wang W. *Macromolecules*, **2011**, *44*, 2410-2414.
13. Zhang C.; Zhu P.-C.; Tan L. *Macromolecules*, **2015**, *48*, 8509-8514.

14. Song K.; Zou Z.; Wang D. *The Journal of Physical Chemistry C*, **2016**, *120*, 2187-2197.
15. Saleh M.; Lee H. M.; Kemp K. C. *ACS Applied Materials & Interfaces*, **2014**, *6*, 7325-7333.
16. Chen Q.; Liu D.-P.; Luo M. *Small*, **2014**, *10*, 308-315.
17. Zhang X.; Lu J.; Zhang J. *Chemistry of Materials*, **2014**, *26*, 4023-4029.
18. Jiang F.; Jin T.; Zhu X. *Macromolecules*, **2016**, *49*, 5325-5330.
19. Luo J.; Zhang X.; Zhang J. *ACS Catalysis*, **2015**, *5*, 2250-2254.
20. Jin T.; Xiong Y.; Zhu X. *Chemical Communications*, **2016**, *52*, 4454-4457.
21. Yuan Y.; Huang H.; Chen L. *Macromolecules*, **2017**, *50*, 4993-5003.
22. Zhang R.-R.; Yin Q.; Liang H.-P. *Polymer*, **2018**, *143*, 87-95.
23. Qiao S.; Li Z.; Zhang B. *Microporous and Mesoporous Materials*, **2019**, *284*, 205-211.
24. Yin Q.; Chen Q.; Lu L.-C. *Beilstein Journal of Organic Chemistry*, **2017**, *13*, 1212-1221.
25. Wang T.; Zhao Y.-C.; Zhang L.-M. *Beilstein Journal of Organic Chemistry*, **2017**, *13*, 2131-2137.
26. Thirion D.; Lee J. S.; Özdemir E. *Beilstein Journal of Organic Chemistry*, **2016**, *12*, 2274-2279.
27. Samanta P.; Chandra P.; Ghosh S. K. *Beilstein Journal of Organic Chemistry*, **2016**, *12*, 1981-1986.
28. Lang M.; Schade A.; Bräse S. *Beilstein Journal of Organic Chemistry*, **2016**, *12*,

- 2570-2576.
29. Cantín Á.; Gomez M. V.; De La Hoz A. *Beilstein Journal of Organic Chemistry*, **2016**, *12*, 2181-2188.
30. Zhang B.; Yan J.; Li G. *Polymer Chemistry*, **2019**,
31. Su H.; Du Y.; Zhang J. *ACS Applied Materials & Interfaces*, **2018**, *10*,
32828-32837.
32. Zhou J.-X.; Luo X.-S.; Liu X. *Journal of Materials Chemistry A*, **2018**, *6*,
5608-5612.
33. Sing, K. S. W. *Pure and Applied Chemistry*, **1985**, *57*, 603-620.
34. Fu H.-X.; Zhang Z.-H.; Fan W. *Journal of Materials Chemistry A*, **2019**, *7*,
15048-15053.
35. Zhang A. J.; Gao H.; Li W. Q. *Polymer*, **2016**, *101*, 388-394.
36. Deka N.; Deka J.; Dutta G. K. *ChemistrySelect*, **2018**, *3*, 8483-8490.
37. Xiang Z.; Mercado R.; Huck J. M. *Journal of the American Chemical Society*,
2015, *137*, 13301-13307.
38. Madani S. H.; Rodríguez-Reinoso F.; Biggs M. J. *Journal of Chemical &
Engineering Data*, **2018**, *63*, 3107-3116.